

# Production, calibration, and performance of the layer 1 replacement modules for the CMS pixel detector

Dinko FERENČEK<sup>1\*</sup>, Matej ROGULJIĆ<sup>1</sup>, and Andrey STARODUMOV<sup>1,2</sup> for the CMS Tracker Group

<sup>1</sup>*Ruđer Bošković Institute, 10000 Zagreb, Croatia*

<sup>2</sup>*Institute for Theoretical and Experimental Physics, Moscow, Russia*

\*E-mail: [Dinko.Ferencek@irb.hr](mailto:Dinko.Ferencek@irb.hr)

(Received December 10, 2020)

The layer 1 modules of the CMS pixel detector at the LHC will be substituted with new ones during long shutdown 2 in 2021. An improved readout chip is used to build these modules. Module production took place in 2020. In this report we describe the module assembly, quality assurance and calibration procedures. Performance of the modules obtained in electrical tests under controlled temperature and humidity as well as under high-rate X-ray irradiation is presented. The production, quality assurance, and calibration of the replacement modules has been successfully completed with the final production yield of 78%. The replacement modules are mounted on the layer 1 support structure.

**KEYWORDS:** CMS pixel detector, CMS Phase-1 upgrade, silicon sensor, readout chip, high density interconnect, silicon pixel detector, hybrid pixel module

## 1. Introduction

The Phase-1 upgraded pixel detector (see Fig. 1) was installed during the extended year-end technical stop (EYETS) 2016/17. Due to radiation damage, the innermost layer

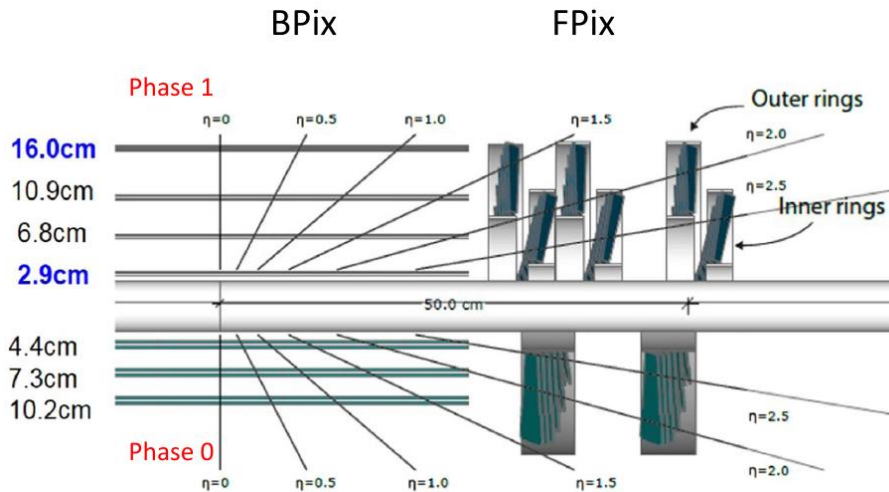


**Fig. 1.** Layout of the original (Phase 0) and upgraded (Phase 1) pixel detector, in  $r$ - $z$  view.

(L1) of the pixel barrel detector (BPix) would have to be replaced during Run 3 [1, 2]. To avoid such a scenario, a replacement for L1 has been built now during long shutdown 2 (LS2) of the LHC and will be installed before Run 3 starts. Building the L1 replacement is a joint project of Paul Scherrer Institute (PSI), ETH Zürich, Helsinki Institute of Physics (HIP), and Ruđer Bošković Institute (RBI). The RBI team's main task was to perform a complete qualification and calibration of about 140 pixel modules. The final goal is to produce 96 installable modules (the total number of modules in L1) with an additional 20% spares.

## 2. L1 Module Overview

The core component of the pixel module, shown in Fig. 2, is an  $n^+$ -in- $n$  silicon sensor with an active area of  $16.2 \times 64.8 \text{ mm}^2$  and comprising 66,560 pixels. It is sandwiched in between 16 readout chips (ROCs) and a very thin PCB, the High Density Interconnect (HDI). The HDI is glued on top of the sensor and wire-bonded to ROCs. The HDI distributes low and high voltages, clock and trigger signals, and routes data between ROCs and two Token Bit Manager (TBM) ASICs. The TBMs organize the readout by aggregating and formatting the data received from ROCs. ROCs are bump-bonded to the sensor and their role is to read and process signals from the sensor. Pixel modules used in building of the L1 replacement feature improved versions of the ROC (PROC600 v4) and TBM (TBM10d) [2]. In particular, TBM10d was designed to be more robust against single event upset (SEU) effects.

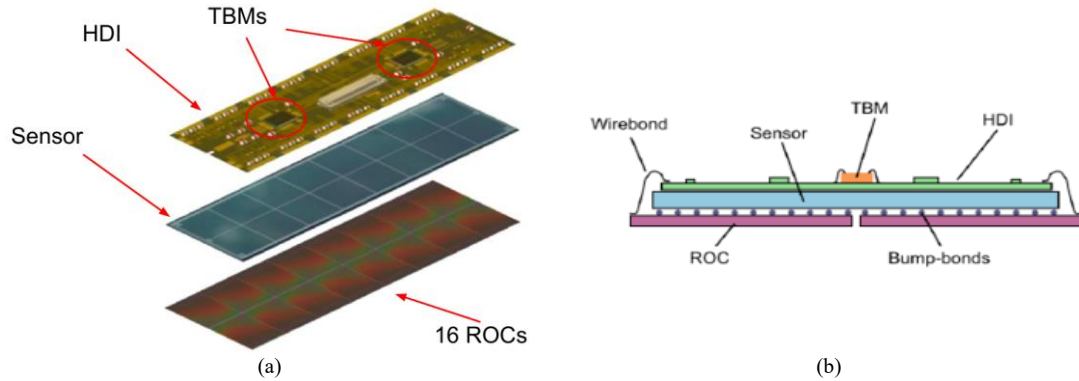


**Fig. 2.** (a) Exploded view of the L1 pixel module with its main components shown. (b) Side view of the fully assembled L1 pixel module.

### 3. Test Setup and Procedures

The full qualification and calibration of pixel modules is done using the cold box setup at PSI shown in Fig. 3. Modules are mechanically stressed through five thermal

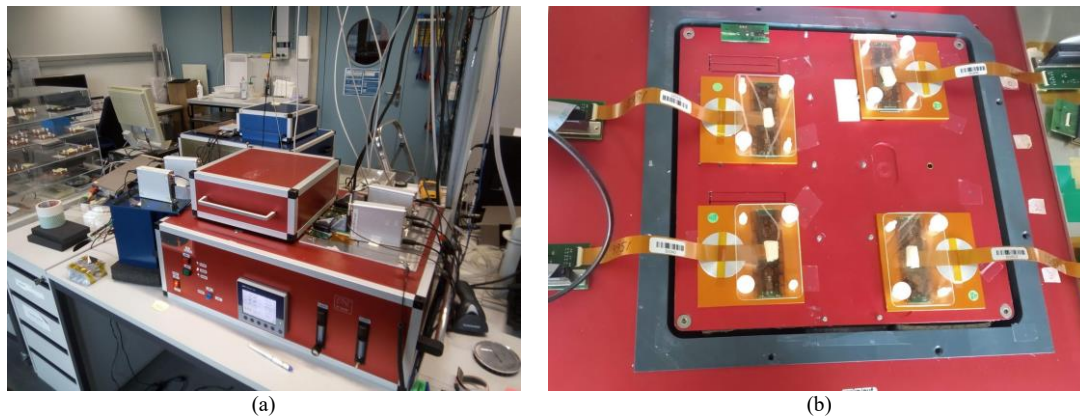


**Fig. 3.** (a) Cold box test setup located in the pixel detector lab at PSI. (b) Inside of the top compartment of the cold box which can house up to four pixel modules and once closed provides a temperature and humidity controlled environment for module tests.

cycles between  $-20\text{ }^{\circ}\text{C}$  and  $+10\text{ }^{\circ}\text{C}$ . Electrical tests and calibration are performed at  $-20\text{ }^{\circ}\text{C}$  both before and after the thermal cycling as well as at  $+10\text{ }^{\circ}\text{C}$  after the warm-up. The full test sequence takes about 8 hours to complete. The current-voltage characteristic (IV-curve) is measured at both  $-20\text{ }^{\circ}\text{C}$  and  $+10\text{ }^{\circ}\text{C}$ . Modules are also tested and calibrated using the X-ray setup at ETH Zürich shown in Fig. 4 where up to two modules can be tested in parallel. The most important test is the measurement of the module performance at an X-ray rate of  $300\text{ MHz/cm}^2$  which is equivalent to the expected hit rate in L1 at the LHC. In particular, the hit efficiency of a single pixel is measured by sending a number  $N$  of internal calibration pulses to that pixel in the presence of X-rays and counting the number of successful readouts  $N_r$ . The single pixel hit efficiency is defined as the ratio

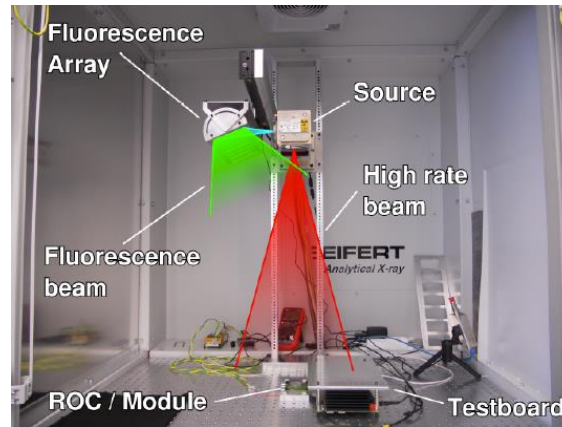


**Fig. 4.** X-ray test setup at ETH Zürich. The direct beam from the X-ray source is used for high rate efficiency measurements while the secondary beam from the fluorescence target is used for the calibration of the ROC response.

$N_r/N$ . The energy calibration is performed using the X-ray fluorescence from four different targets (Zn, Mo, Ag, and Sn). Known energy levels of each target allow the ROC response to be calibrated in electrons. The test and analysis software as well as the grading criteria are mostly inherited from the original Phase-1 production campaign with some updates and/or extensions where needed [2, 3]. In particular, the grading criteria had to be updated to accommodate characteristics of the improved ROC.

#### 4. Module Performance

The performance of tested pixel modules is summarized in Figs. 5–7. Pixel thresholds are trimmed to about 2000  $e^-$  and show an excellent uniformity to within about 40  $e^-$  and are stable as a function of temperature. The mean noise at  $-20^\circ\text{C}$  is around 200  $e^-$  with a small tail to higher values. Under X-rays the noise increases and a significant tail to higher values appears. Unlike in the cold box tests, where pixels are enabled one at a time, under

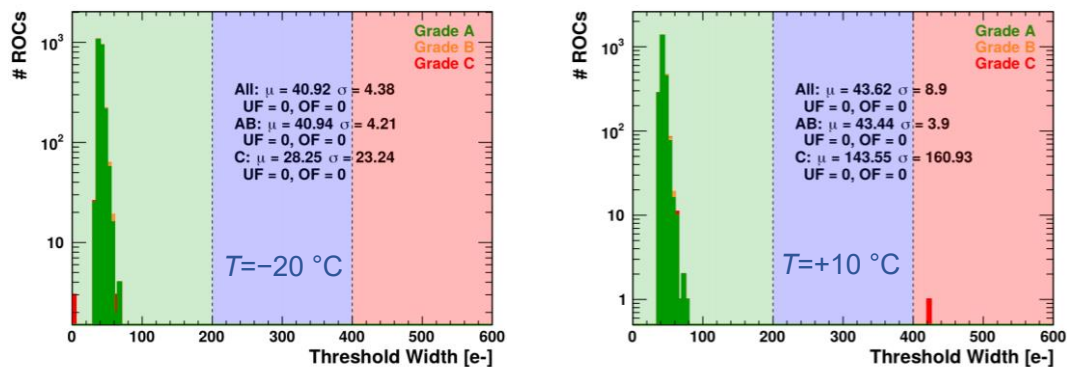


**Fig. 5.** ROC threshold width distributions after the procedure of equalizing the physical threshold of the single pixels called trimming at  $-20^\circ\text{C}$  (left) and  $+10^\circ\text{C}$  (right) for ROCs of different grades. UF and OF in the legend refer to the number of underflow and overflow entries, respectively.

X-rays all pixel are enabled and the channel cross-talk is causing higher levels of noise. A great majority of ROCs have the hit efficiency above 98% which is the target value for PROC600.

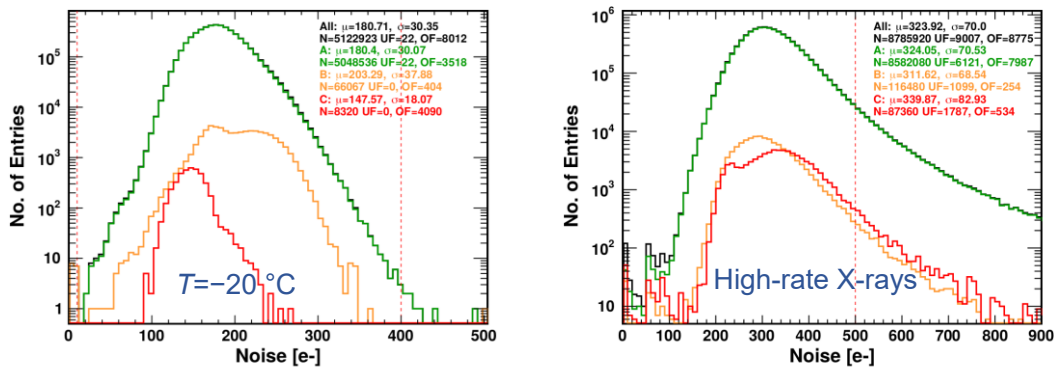


Fig. 6. Noise per pixel distributions at  $-20\text{ }^{\circ}\text{C}$  (left) and under high-rate X-rays (right) for ROCs of different grades. UF and OF in the legend refer to the number of underflow and overflow entries, respectively.

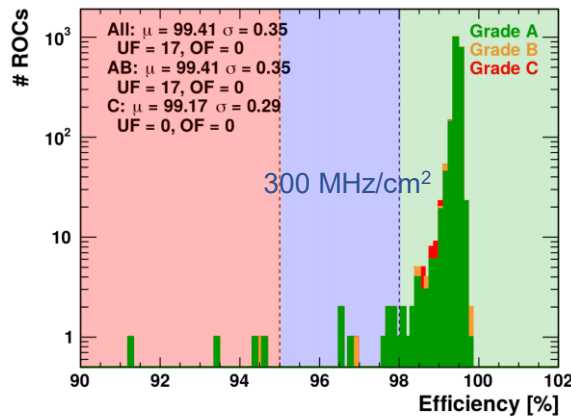


Fig. 7. ROC hit efficiency distributions measured using internal calibration pulses at an X-ray rate of  $300\text{ MHz/cm}^2$  for ROCs of different grades. UF and OF in the legend refer to the number of underflow and overflow entries, respectively.

Modules are graded based on the number of defective (broken or noisy) pixels, the hit efficiency, the leakage current as well as other parameters. The full list of parameters [4] and the grading criteria are summarized in Table I. The final module grade is based on the grade of the worst performing ROC in that module. Both grade A and B modules are installable.

**Table I.** The full list of parameters entering the module grading and the grading criteria.

Parameter	Grade		
	A	B	C
ROC grading			
Mean noise	<200 e <sup>-</sup>	<300 e <sup>-</sup>	>300 e <sup>-</sup>
Threshold width	<200 e <sup>-</sup>	<400 e <sup>-</sup>	>400 e <sup>-</sup>
Relative gain width	<0.1	<0.2	>0.2
Pedestal spread	<2500 e <sup>-</sup>	<5000 e <sup>-</sup>	>5000 e <sup>-</sup>
Fraction of defective pixels	<1%	<4%	>4%
Sensor grading			
$I_{leak} (T=+10\text{ }^{\circ}\text{C})$	<2 μA	<10 μA	>10 μA
X-ray grading			
Efficiency at 300 MHz/cm <sup>2</sup>	>98%	>95%	<95%
Column uniformity problems	0	0	≥1
Readout uniformity problems	0	0	≥1
Fraction of defective pixels	<1%	<4%	>4%

A cumulative module production graph is shown in Fig. 8 and the module grading summary is shown Table II. Modules marked as “Faulty after assembly” could not be subject to any of the tests due to module communication or initialization problems. Modules for which tests are marked as “Incomplete” failed an initial set of basic functionality tests and are therefore excluded from any of the subsequent tests. Only modules with grades A or B from the full qualification are subject to the high-rate test. The final production yield, defined as the ratio of the number of grade A and B modules to the total number of modules, is  $(A+B)/Total=110/141=78\%$ .

The installable modules are finally ranked based on their quality and assigned to appropriate locations on the L1 support structure (higher quality modules closer to the center). The replacement modules mounted on the L1 support structure are shown in Fig. 9.

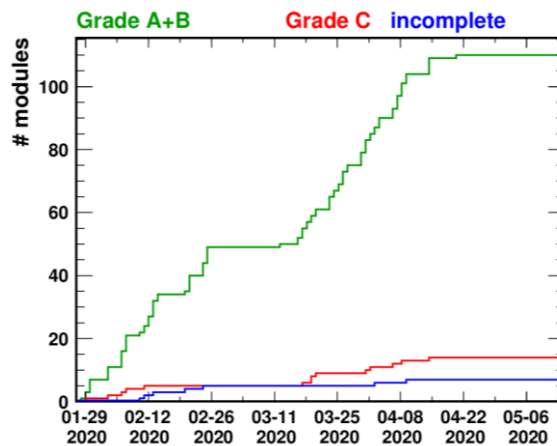


**Fig. 8.** Cumulative production graph for modules of different grades.

**Table II.** Module grading summary.

	Grade			Total
	A	B	C	
Faulty after assembly	-	-	-	10
Incomplete	-	-	-	5
Full qualification	13	110	3	126
High-rate test	87	24	12	123
Final	8	102	14	141

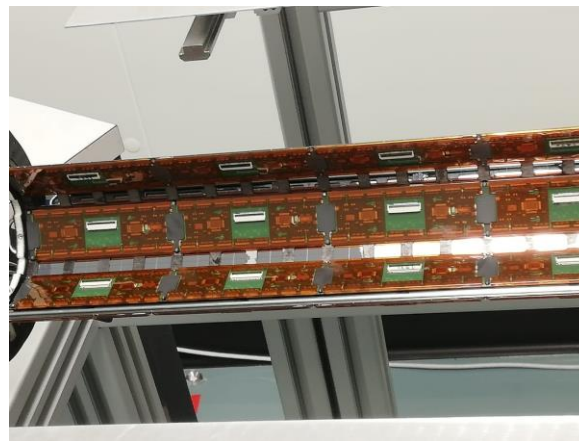


**Fig. 9.** Modules mounted on a L1 half-shell.

## 5. Summary

The production, quality assurance, and calibration of the L1 replacement modules for the CMS pixel detector has been successfully completed with the final production yield of 78%. The replacement modules are mounted on the L1 support structure.

## Acknowledgment

We would like to thank our colleagues from PSI (Wolfram Erdmann, Hans-Christian Kästli, Danek Kotlinski, Urs Langenegger, Beat Meyer, Tilman Rohe, Silvan Streuli), ETH Zürich (Malte Backhaus, Maren Meinhard, Franz Glessgen, Krunal Gedia, Branislav Ristic, Vasilije Perovic), and HIP (Erik Brücken, Panja Luukka, Akiko Gädda, Shudhashil Bharthuar, Raimo Turpeinen, and Pirkitta Koponen) who were involved in different stages of the production and testing of the replacement modules. We would especially like to thank the PSI group for their hospitality during our stays at PSI.

This work was supported in part by the Croatian Science Foundation, under the

project IP-2016-06-3321, by the European Union's Horizon 2020 research and innovation programme, under grant agreement No 669014 (PaRaDeSEC), and by the European Union's European Regional Development Fund.

## References

- [1] A. Dominguez et al. for the CMS Collaboration, CMS Technical Design Report for the Pixel Detector Upgrade, CMS-TDR-011, URL: <https://cds.cern.ch/record/1481838>
- [2] The Tracker Group of the CMS Collaboration, The CMS Phase-1 Pixel Detector Upgrade (submitted to JINST)
- [3] K. Klein for the CMS Collaboration, The Phase-1 upgrade of the CMS pixel detector, Nucl. Instrum. Meth. A **845** (2017) 101-105, DOI: [10.1016/j.nima.2016.06.039](https://doi.org/10.1016/j.nima.2016.06.039)
- [4] Section 9 in Vittorio Tavaloro's PhD thesis, DOI: [10.3929/ethz-b-000337242](https://doi.org/10.3929/ethz-b-000337242), URL: <https://www.research-collection.ethz.ch/handle/20.500.11850/337242>